A&A 460, 459–466 (2006)
DOI: 10.1051/0004-6361:20054132

Astronomy & Astrophysics

Properties of RR Lyrae stars in the inner regions of the Large Magellanic Cloud

II. The extended sample⋆,⋆⋆

J. Borissova[1], D. Minniti[2], M. Rejkuba[3], and D. Alves[4]

[1] Departamento de Física y Meteorología, Facultad de Ciencias, Universidad de Valparaíso, Ave. Gran Bretaña 644, Playa Ancha, Casilla 53, Valparaíso, Chile
e-mail: jura.borissova@uv.cl
[2] Department of Astronomy, P. Universidad Católica, Av. Vicuña Mackenna 4860, Casilla 306, Santiago 22, Chile
e-mail: dante@astro.puc.cl
[3] European Southern Observatory, Karl-Schwarzschild-Str. 2, 85748 Garching b. München, Germany
e-mail: mrejkuba@eso.org
[4] 3549 Lynne Way, Sacramento, CA 95821-3722, USA
e-mail: alvesdavid@ucdavis-alumni.com

Received 31 August 2005 / Accepted 17 August 2006

ABSTRACT

Context. All galaxies that have been adequately examined so far have shown an extended stellar halo.
Aims. To search for such a halo in the LMC we have obtained low-resolution spectra for 100 LMC RR Lyrae stars, of which 87 are in the field and 13 in the clusters NGC 1835 and NGC 2019.
Methods. We measured radial velocities for 87 LMC RR Lyrae stars, and metallicities for 78 RR Lyrae stars, nearly tripling the previous sample. These targets are located in 10 fields covering a wide range of distances, out to 2.5 degrees from the center of the LMC.
Results. Our main result is that the mean velocity dispersion for the LMC RR Lyrae stars is $\sigma_{RV} = 50 \pm 2$ km s^{-1}. This quantity does not appear to vary with distance from the LMC center. The metallicity shows a Gaussian distribution, with mean [Fe/H] = -1.53 ± 0.02 dex, and dispersion $\sigma_{[Fe/H]} = 0.20 \pm 0.02$ dex in the Harris metallicity scale, confirming that they represent a very homogeneous metal-poor population. There is no dependence between the kinematics and metallicity of the field RR Lyrae star population.
Conclusions. Using good quality low-resolution spectra from FORS1, FORS2 and GEMINI-GMOS we have found that field RR Lyrae stars in the LMC show a large velocity dispersion and that this indicate the presence of old and metal-poor stellar halo. All the evidence so far for the halo, however, is from the spectroscopy of the inner LMC regions, similar to the inner flattened halo in our Galaxy. Further study is necessary to confirm this important result.

Key words. galaxies: structure – stars: variables: RR Lyrae – Magellanic Clouds – stars: kinematics

1. Introduction

The LMC is an irregular, disk dominated, bulge-less, nearly face-on galaxy. It is of fundamental importance for studies of stellar populations and of the interstellar medium. It is being used to study the presence of dark objects in the Galactic Halo through microlensing (e.g., Alcock et al. 2000a,b), it is an important probe of the Galaxy's formation history, and it plays a key role in determinations of the cosmological distance scale (e.g., Freedman et al. 2001).

All galaxies that have been adequately examined so far have shown an extended star halo. Furthermore the Lambda CDM cosmology predicts a dark matter halo for galaxies like the LMC. Unfortunately, outlining a stellar halo in the LMC (and its metal and age distribution), a key observation for galaxy formation scenarios, is made difficult by the large extent of this galaxy on the sky and inclination, causing the halo to be projected against the LMC disk.

Recently, using low resolution spectroscopy with the FORS1 spectrograph at the Very Large Telescope (VLT), Minniti et al. (2003) and Borissova et al. (2004; hereafter Paper I) on the basis of the radial velocities of 43 RR Lyrae stars obtained a true velocity dispersion of 53 km s^{-1}, which is higher than the velocity dispersion of any other LMC population previously measured. This high velocity dispersion indicates that a kinematically hot metal-poor old halo exists in the LMC.

Cole et al. (2005) reported metallicities and radial velocities derived from spectra at the near-infrared calcium triplet for 373 red giants in a 200 arcmin^2 area at the optical center of the LMC bar. They found that the velocity dispersion of the whole sample is 24.7 ± 0.4 km s^{-1}. When cut by metallicity, the most metal-poor 5% of stars ([Fe/H] < −1.15) show 40.8 ± 1.7 km s^{-1}, more

⋆ Based on observations collected with the Very Large Telescope, the New Technology Telescope of the European Southern Observatory and GeminiS of Gemini Observatory within the Observing Programs 64.N-0176(B),70.B-0547(A), 072.D-0106(B), GS-2004A-Q-27.
⋆⋆ Table 9 is only available in electronic form at http://www.aanda.org

Table 1. The centers of the observed fields. The log of the observations.

Event	RA	Dec	Instrument	Date of obs.	Exp. time (min)	No of Exp.	RRLyr's	Cep's	LPVs
LMC-4	05:17:14.6	–70:46:59.0	FORS2	28.12.2003	20	2	14	1	0
LMC-9	05:20:20.3	–69:15:12.0	FORS2	28.12.2003	20	2	18	3	8
LMC-14	05:34:44.0	–70:25:07.0	FORS2	28.12.2003	20	2	14	0	3
LMC-18	05:45:21.1	–71:09:11.2	FORS2	28.12.2003	20	2	2	0	4
Ne01	05:18:01.0	–69:29:53.0	FORS2	28.12.2003	20	2	18	6	0
LMC-F1	05:28:28.4	–69:33:48.8	GMOS	17.03.2004	30	2	8	0	6
LMC-F2	05:37:19.2	–70:00:39.0	GMOS	20.03.2004	30	2	6	0	7
LMC-F4	05:05:35.0	–68:44:45.7	GMOS	22.03.2004	30	2	7	0	9
NGC1835	05:05:07.1	–69:24:14.2	GMOS	27.03.2004	30	2	11	0	0
NGC2019	05:31:56.5	–70:09:32.5	GMOS	19.04.2004	30	2	2	0	13

than twice the value for the most metal-rich suggesting that an old, thicker disk or halo population is present, in agreement with our results from RR Lyrae stars.

It is impossible for the LMC halo to be spherical in the outer regions according to Alves (2004), who re-examined the content of the 2MASS database at its periphery, up to 12 degrees from the center. Based on the dereddened colors of the LMC's red giant branch (RGB) stars, he found an outward radial gradient of decreasing metallicity (an increasing percentage of metal-weak stars comparable to RR Lyrae). In a novel mathematical analysis, he showed that the center of symmetry of the isodensity contours of the RGB stars at the periphery is North-East of the center indicated by the maximum of the isodensity of RR Lyrae stars; this discrepancy of centers rules out a spherical halo. The contrast with the sphericity of the LMC halo revealed by the kinematics of RR Lyrae stars may be best interpreted as a unique observation of galaxy halos.

Other evidence from photometric data was presented by Gallart et al. (2004) from a high-quality color-magnitude diagram (CMD) for a 36×36 arcmin field located at 7 kpc from the LMC center. The surface brightness profile of the LMC remains exponential to this large galactocentric radius and shows no evidence of disk truncation. Combining the information on surface brightness and stellar population, they concluded that the LMC disk extends (and dominates over a possible stellar halo) out to a distance of at least 7 kpc. Clementini et al. (2003) and Gratton et al. (2004) presented new photometry and spectroscopy for more than a hundred RR Lyrae stars in two fields located close to the bar of the LMC. Their average magnitude, the local reddening, individual metallicities, the luminosity-metallicity relation, and the distance to the LMC were derived. They calculated the dispersion of the mean radial velocity of the 48 stars with multiple observations of 40 km s^{-1}.

Subramaniam (2006) investigated the distribution of the RR Lyrae star population in the inner LMC and found a halo-like location and disc-like density distribution. She also found that RR Lyrae stars in the inner LMC are elongated more along the line of sight than along the major axis of the disk. Thus there are many indications that the LMC has a halo, which is similar to the inner halo of our Galaxy, but the results are puzzling. The outer halo of the LMC, which is characterized by a spatially extended old population with large velocity dispersion, has still not been detected.

In this paper we present new spectroscopic data extending our sample to 137 field RR Lyrae stars and 13 RR Lyrae stars in the LMC globular clusters NGC 1835 and NGC 2019. The next section describes the data and the third section discusses the radial velocities of the extended sample. The fourth section includes the metallicities and the last section is a summary of the results.

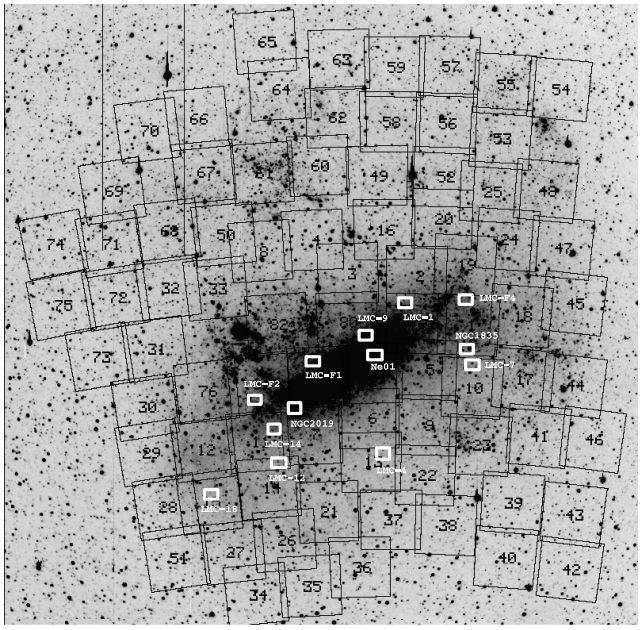

Fig. 1. MACHO image (http://www.macho.mcmaster.ca/) of LMC (*R*-band) showing the location of the MACHO fields and the fields for which we obtained MOS spectra. North is up and east is to the left. The small thick boxes indicate the $7' \times 7'$ field of view of the FORS1/FORS2 CCD images and $6' \times 6'$ GMOS fields.

2. Observations and reductions

In Paper I we presented radial velocities, metallicities and *K*-band magnitudes of 74 RR Lyrae stars in the inner regions of the LMC. The optical low resolution spectra were obtained with the FORS1 at the ESO VLT and near-IR photometry images with the SOFI infrared array at the ESO NTT. We have chosen to extend this sample by using the MACHO (Alcock et al. 2000b) and OGLE (Zebrun et al. 2001) databases to seven fields of the LMC bar, at distances from 0.4 to 2.5 degrees away from the rotation center (Soszynski et al. 2003). Two of these new fields are centered on the LMC clusters NGC 1835 and NGC 2019. We also observed additional stars in the fields LMC-4, LMC-9 and LMC-14 defined in Paper I. As a control sample for the LMC kinematic properties, we have selected known long period variables (LPV) and Cepheids from MACHO and OGLE in the same fields (see also Paper I). The observed fields are summarized in Table 1 and shown in Fig. 1 along with fields observed in Paper I.

The whole sample (including data from Paper I) of RRab stars covers the period interval from 0.46 days to 0.78 days (only one star has a period of 0.97 days), with a mean value of 0.575 ± 0.08 days. The RRc stars' periods range from 0.27

to 0.43 days and the mean period is 0.36 ± 0.04 days. The RRe stars have the mean period 0.28 ± 0.01 days. These values are very similar to the values determined by the MACHO team $\langle P_{ab} \rangle = 0.583$ days (Alcock et al. 1996) from ∼7900 RR Lyrae stars and the recent work of the OGLE team (Soszynski et al. 2003): $\langle P_{ab} \rangle = 0.573$ days. For RRc stars the mean periods are $\langle P_c \rangle = 0.342$ days, from the MACHO team and $\langle P_c \rangle = 0.339$ from the OGLE team.

The new spectroscopic observations were taken with the FORS2 multi-slit spectrograph at the ESO Very Large Telescope (VLT) Unit Telescope 4 (UT4), during the night of 28 December 2003, and with the Gemini South multi object spectrograph (GMOS) in queue mode. We used FORS2 with the GRIS_600B+22 grating that gives $R = 780$ and covers from λ3300 to λ6210 Å. GMOS was used with the B600+G5323 grating, which is centered on λ5000 Å and gives $R = 1688$. The resolution of FORS1 with GRIS_600B+12 is also 780. FORS2 has 19 movable slits, while in GMOS it is possible to put a hundred slits in a single mask. The field of view of GMOS is only 5.5 × 5.5 arcmin, while FORS2 has a field of view 6.8×6.8 arcmin. The seeing during the FORS2 observations was 0.6–0.7 arcsec, while GMOS spectra were taken with the mean seeing of 1 arcsec. Both resolutions are adequate for the measurement of radial velocities even in the broad-lined RR Lyrae star spectra, provided that a sufficient S/N is achieved. During the pulsation of a RR Lyrae variable, the star's radial velocity varies from the systemic velocity. To avoid excessive broadening of spectral lines by changing velocity, the integration times of the spectroscopic observations should be kept under 5 percent of the pulsation cycle. In total, two exposures of 20 min with FORS2 and 30 min with GMOS were obtained for each mask containing 5–10 RR Lyrae stars. We placed LPV and Cepheid variables on the remaining slits. The FORS2 observations were taken in one night but are spaced in time to allow a better sampling of the radial velocity variation with phase. The GMOS observations are taken during 5 different nights.

In this extended sample we observed 100 RR Lyrae stars, 10 Cepheids, and 50 Miras with FORS2 and GMOS.

Using the same setup we also observed RR Lyrae stars of the globular cluster ω Cen with GMOS and repeated observations of some of the RR Lyrae stars in the LMC field, in order to assess the velocity errors.

The spectral data were reduced using the standard packages within IRAF. HeNeAr lamps were used for the wavelength calibration. Each spectrum was individually calibrated using an order 3 cubic spline function for the fit and typically 14 usable lines. The rms of the dispersion solution varies between 0.03 and 0.2 Å rms. The 0.2 Å rms of the wavelength calibration contributes about 12–13 km s^{-1} (at $\lambda \sim 5000$ Å) to the error budget of the individual radial velocity measurements and is added in quadrature to the other error sources.

To check the wavelength calibration, we measured several emission lines of the night sky that were also present in our 20 and 30 min long exposures. The reference wavelengths of these lines were taken from the Keck telescope web page. In fifty six of our spectra we can measure the strong [OI] skyline at 5577.338 Å and in some cases Na I at 5889.950 Å. The central wavelengths of these lines were measured by fitting a Gaussian profile. The mean deviations of sky lines from their reference wavelengths varied from star to star and from −1.18 Å to +0.74 Å. Following Gallart et al. (2001) and Vivas et al. (2005), these deviations were used to correct the zero point of the wavelength scale, which were applied to each spectrum by modifying the header parameter CRVAL1, the starting wavelength. The standard deviation of the mean offset of the sky lines from their reference wavelengths was typically of 0.09 Å (or ∼6 km s^{-1}).

In summary, the daytime lamp spectra are used to determine the dispersion relation, but the zero point of the calibration, when possible is corrected by measuring the wavelengths of the skylines. Because we split the exposure time of each program star in two we extracted, wavelength calibrated and corrected each observation individually. Then, the two spectra were summed to improve the S/N. The final extracted and calibrated spectra have on average $S/N = 30$ for FORS2 and $S/N = 25$ for GMOS at 4750 Å for LMC RR Lyrae stars. The S/N ratio for each star is given in Col. 4 of Table 9.

3. Radial velocities

The radial velocities of the stars were measured with the IRAF task fxcor, which performs a Fourier cross-correlation between a program star and a radial velocity standard star. The wavelength range for the cross-correlation was from 3800 to 5250 Å, which includes hydrogen lines (Hϵ, Hβ, Hγ and Hδ) and Ca II K λ 3933.66 Å. As expected with the high S/N of our spectra, the correlation peaks were well defined in all cases. However, they were broad because the correlations are dominated by the Balmer lines, which are wide features in these stars with A-F type spectra. Since the cross-correlation has to be made with a template that has a spectral type similar to the targets and we did not observe any radial velocity standard during our runs, we retrieved from the ESO archive the radial velocity standards Kopff 27(A3 V), Feige 56 (A0 V) and HD 155967(F6 V). They were taken with the same instrument and setup (FORS2, GRIS_600B+22 grating, 1 arcsec wide slit) under program 069.B-0343 (PI: Gallart). The spectra of these stars were reduced in the same way as the program stars, including a zero point correction with the skylines. After careful inspection we chose to use as a template star HD 155967, because its spectrum has the highest S/N. Each spectrum of RR Lyrae star was therefore correlated with the spectrum of this standard.

3.1. Error analysis

While fxcor returns a value for the standard deviation of the cross-correlation, this is not a true measure of the uncertainty because it does not take into account the zero-point uncertainty in the wavelength calibrations of the program star and the standard star. The sigmas of these zero-points were therefore added in quadrature to this value. For fifty six stars we added in quadrature the zero point corrections of the program stars plus the zero point correction of the HD 155967 (0.02 Å), and for the remaining stars, which have no measurable skylines in their spectra, we added the conservative estimate of 15 km s^{-1}. These final errors are listed in Col. 3 of Table 9. Their mean value is 25 ± 1 km s^{-1}.

To check the estimate of the observational errors and homogeneity of the sample we compared the results obtained from multiple observations of some stars. There are 11 LMC RR Lyrae stars observed with FORS1 and FORS2 with four spectra. They are given in the first eleven rows of Table 2. The standard deviation of the measured velocities of these stars is in the range from 2 to 35 km s^{-1}, with a mean value of 18 ± 3 km s^{-1}. The remaining thirty stars in the same table are RR Lyrae stars observed with GMOS on different nights, with 30 min exposures, which have a high enough signal to noise ratio to measure the radial velocities on the individual, not summed spectra. The mean

Table 2. LMC RR Lyrae common stars observed with FORS1, FORS2 and GMOS.

Name	$\langle V \rangle$	RV_1	RV_2	$RV_{\rm MEAN}$	σ_{RV}
MACHO79.5508.735	19.78	246	289	268	30
MACHO13.5960.884	19.23	226	223	225	2
MACHO13.5961.623	19.24	261	300	281	28
MACHO13.5962.547	19.21	283	275	279	6
MACHO13.5962.656	19.34	271	305	288	24
MACHO80.6469.1657	19.24	218	195	207	16
OGLE052013.42-691153.0	18.97	177	212	195	25
OGLE052026.29-691815.0	19.12	199	248	224	35
MACHO11.8871.1122	19.71	261	250	256	8
MACHO11.8871.1299	19.61	271	282	277	8
MACHO11.8871.1447	19.59	156	178	176	16
OGLE052829.20-693201.1	19.30	146	152	149	4
OGLE052822.98-693310.6	19.40	327	310	319	12
OGLE052827.10-693347.7	20.06	191	205	198	10
OGLE052834.72-693326.4	19.37	125	173	149	34
OGLE052811.62-693423.8	19.50	290	352	321	44
OGLE052829.28-693442.0	19.80	217	287	252	49
OGLE052854.41-693403.8	19.40	150	217	184	47
OGLE052822.65-693529.9	19.42	299	308	304	6
OGLE053720.10-700202.5	19.51	268	313	291	32
OGLE053715.52-695812.2	20.08	208	220	214	8
OGLE053714.30-695846.0	20.00	229	326	278	69
OGLE053717.79-695923.9	19.57	189	167	178	16
OGLE053713.07-695956.8	19.98	272	267	270	4
OGLE053715.59-700105.8	21.00	210	291	251	57
OGLE050516.31-684514.9	19.41	326	351	339	18
OGLE050542.14-684529.5	19.42	305	323	314	13
OGLE05054491-6844330.0	19.30	320	317	319	2
OGLE050519.07-684522.5	18.41	324	350	337	18
OGLE050516.31-684514.9	19.41	305	359	332	38
OGLE050509.55-692505.5	19.04	248	209	229	28
OGLE050505.88-692500.9	19.30	207	228	218	15
OGLE050456.54-692449.0	20.00	114	174	144	42
OGLE050457.92-692419.2	19.35	203	223	213	14
OGLE050458.96-692447.2	19.20	197	195	196	1
OGLE050514.52-692412.2	19.37	186	247	217	43
OGLE050512.73-692446.5	19.32	131	189	160	41
OGLE050507.42-692346.6	19.26	153	225	189	51
OGLE050501.95-692343.5	19.31	191	186	189	4
OGLE050508.49-692330.7	19.20	213	212	213	1
OGLE050503.49-692319.2	19.61	182	216	199	24

value of the dispersion of these stars is 25 ± 4 km s^{-1}. The whole sample of 41 stars has a mean dispersion of 23 ± 3 km s^{-1}. Table 2 lists the radial velocities of the common stars.

During the pulsation of a typical ab RR Lyrae variable, the star's radial velocity varies by ± 50–60 km s^{-1} about the systemic velocity (Layden 1994). In order to estimate the influence of the pulsation of the stars on the velocity dispersion we performed the following test. We selected eighteen RR Lyrae stars observed with GMOS with the best quality spectra and measured their radial velocities from the individual, not summed spectra. The OGLE and MACHO databases were used to derive the phases of the stars at the time of our observations. As in Vivas et al. (2005) we fitted each star with the radial velocity curve of the well-studied RR Lyrae star X Arietis to calculate the systemic velocity. We used Layden's (1994) parameterization of the velocity curve that Oke (1966) measured from the Hγ line. Following the discussion given in Vivas et al. (2005) and Layden (1994) the Balmer line curves are more appropriate for our purpose than the measurements based on the weak metal lines. The observations at phases less than 0.1 or greater than 0.85 were excluded from our test. In this way we rejected only one star which had phases 0.94 and 0.04. Then we calculated the systemic velocity at phase 0.50 for these stars. The mean value of these seventeen RR Lyrae stars calculated as an average of the two measurements of the radial velocities and the mean value of the systemic velocities do not differ much. The same is true for the respective dispersions. The mean value and dispersion of the averaged two measurements is $RV = 255 \pm 65$ km s^{-1}, while the mean and dispersion of the systemic velocities is $RV = 263 \pm 63$ km s^{-1}. The result is not surprising because for each star we have at least two observations, taken at random phase, which we averaged. The mean error between the average values of the individual radial velocities and systemic ones in our test sample is 9 ± 1 km s^{-1}. Since the mean radial velocity of the test sample and its dispersion are not very sensitive to the pulsation correction and following the analysis from Paper I we decided to use radial velocities of RR Lyrae stars uncorrected for pulsation.

Taking into account all the error estimates described above the upper limit of accuracy of our radial velocity measurements is 25 km s^{-1}. This value is in good agreement with the Gratton et al. (2004) estimates for 48 stars with multiple observations. We have to add in quadrature a conservative estimate of

Table 3. LPV stars from MACHO and OGLE databases observed with FORS2 and GMOS.

Name	V	RV (km s^{-1})	Instrument
OGLE05451038-7107080	14.97	225	FORS2
OGLE05452789-7106578	13.88	309	FORS2
OGLE05453011-7108405	16.21	187	FORS2
OGLE05452114-7110446	15.24	277	FORS2
OGLE05345471-7023475	14.65	217	FORS2
OGLE05344660-7025053	15.36	224	FORS2
OGLE05344085-7026341	19.2	249	FORS2
OGLE05202129-6912571	17.37	226	FORS2
OGLE05201078-6912417	14.99	235	FORS2
OGLE05202110-6914527	16.16	228	FORS2
OGLE05203074-6916455	19.85	193	FORS2
OGLE05201078-6912417	14.99	214	FORS2
OGLE05202948-6914132	17.64	199	FORS2
OGLE05201941-6914598	14.83	232	FORS2
OGLE05202789-6915096	15.88	227	FORS2
OGLE05283307-6931278	14.6	224	GMOS
MACHO 77. 7795. 15	-	243	GMOS
OGLE05280312-6932386	14.65	286	GMOS
OGLE05285235-6933316	14.29	241	GMOS
OGLE05373007-6958385	15.52	227	GMOS
OGLE05372274-6958227	14.11	229	GMOS
OGLE05370332-7000121	16.85	283	GMOS
OGLE05370996-7000013	14.95	277	GMOS
OGLE05365681-6959455	14.09	259	GMOS
OGLE05373747-7001004	16.1	258	GMOS
OGLE05370850-7002122	15.46	267	GMOS
OGLE05372590-7002233	16.73	246	GMOS
OGLE05371190-7002342	14.86	288	GMOS
OGLE05060079-6843090	15.57	223	GMOS
OGLE05055136-6843482	14.82	255	GMOS
OGLE05054684-6843166	14.44	311	GMOS
OGLE05054561-6842581	15.08	258	GMOS
OGLE05055189-6844484	16.09	249	GMOS
OGLE05050860-6844561	16.64	222	GMOS
OGLE05060079-6845587	14.44	258	GMOS
OGLE05055576-6846385	14.82	282	GMOS
OGLE05054263-6846535	14.82	226	GMOS
OGLE05322110-7008233	18.63	291	GMOS
OGLE05314921-7008542	15.66	304	GMOS
OGLE05320041-7008436	14.86	225	GMOS
OGLE05301729-7007148	13.69	228	GMOS
OGLE05300027-7008333	13.77	248	GMOS
OGLE05314492-7008059	14.74	259	GMOS
OGLE05320099-7009133	14.63	255	GMOS
OGLE05315279-7009320	15.2	222	GMOS
OGLE05315958-7010145	18.77	294	GMOS
OGLE05315215-7010026	16.24	301	GMOS
OGLE05321820-7009425	14.92	246	GMOS
OGLE05321906-7009571	17.84	247	GMOS
OGLE05315209-7011096	14.46	270	GMOS

9–10 km s^{-1} from the phase correction, so the final velocity dispersion has to be corrected with $(\sigma^2_{\rm rms} + \sigma^2_{\rm phase})^{-1/2} = 27$ km s^{-1}.

3.2. Kinematics

The data for the OGLE and MACHO LPVs and Cepheids are given in Tables 3 and 4, respectively. The properties of the LMC RR Lyrae stars are summarized in Table 9, where in Cols. 6, 7 and 8 we list the mean V magnitude, period of the pulsation and type of star taken from the MACHO and OGLE database. Radial velocities are shown in Col. 2 and metallicities in Col. 5. These are discussed below.

In summary, the whole dataset (FORS1, FORS2 and GMOS) contains 26 RR Lyrae stars in ω Cen, 73 LPV variable stars, 12 Cepheids, 137 RR Lyrae stars in the field of LMC and 13 RR Lyrae stars in the LMC globular clusters NGC 1835 and NGC 2019.

Following the method described in Minniti et al. (2003) we calculated the dispersions for the velocity measurements for the field RR Lyrae stars, cluster RR Lyrae stars, LPVs and Cepheid stars. They are given in Table 5. The true velocity dispersions of LMC Cepheid and LPV stars are taken from the literature (see Paper I for more details.)

Since we measured $\sigma_{\rm obs} = 57 \pm 3$ km s^{-1} for the LMC field RR Lyrae stars and assuming $(\sigma^2_{\rm rms} + \sigma^2_{\rm phase})^{-1/2} = 27$ km s^{-1}, we obtain $\sigma_{\rm true} = 50 \pm 2$ km s^{-1}. Here $\sigma_{\rm obs}$ is the observed velocity dispersion, calculated as the standard deviation of the individual velocities from the average value, $\sigma_{\rm rms}$ is the mean error of the individual velocity measurements and $\sigma_{\rm phase}$ is the mean dispersion in the velocities because we observed the stars at a random phase. The errors of the observed and true velocity dispersions were calculated as a standard deviation of the mean values divided by the square root of the number of the stars. Thus we confirm our result from Minniti et al. (2003), that a kinematically hot metal-poor old halo exists in the LMC. The average (mean) radial velocity (RV) derived for the LMC field RR Lyrae stars is $RV = 258 \pm 5$ km s^{-1}, in agreement with the Gratton et al. (2004) value of $RV = 261$ km s^{-1} and with the value of 257 km s^{-1} found for LMC red giants by Cole et al. (2005).

The $\sigma_{\rm obs}$ for RR Lyrae stars of the globular clusters NGC 1835 and NGC 2019 is 28 km s^{-1}, and $\sigma_{\rm true} = 7 \pm 2$ km s^{-1}. Freeman et al. (1983) have shown that the clusters older than about 0.3 Gyr appear to lie in a flat rotating disk whose velocity dispersion is only 15 km s^{-1}. This result for the clusters was confirmed by Schommer et al. (1992).

We measured only 13 RR Lyrae stars in NGC 1835 and NGC 2019 and find that the true velocity dispersion of the cluster RR Lyrae is much smaller than the velocity dispersion of the field RR Lyrae stars. Dubath et al. (1997) measured the core velocity dispersions for 10 old Magellanic globular clusters from integrated-light spectra. For NGC 1835 they reported 10.4 km s^{-1} and 7.5 km s^{-1} for NGC 2019. The velocity dispersion obtained from our 11 RR Lyrae stars of NGC 1835 is $\sigma_{\rm true} = 7$ km s^{-1}. For NGC 2019 we have only 2 stars and it is not possible to calculate a realistic value. The average radial velocity derived for the NGC 1835 RR Lyrae stars is $RV = 198 \pm 6$ km s^{-1}, while for the NGC 2019 we obtained 231 ± 2 km s^{-1} from two stars, again in agreement with the average value measured for these clusters by Freeman et al. (1983) and Schommer et al. (1992).

For the 73 LPV stars in the LMC we obtained a mean radial velocity $RV = 252 \pm 5$ km s^{-1} and observed velocity dispersion of 35 ± 3 km s^{-1}.

To test the accuracy and stability of the velocity dispersion measurements we calculated the observed values at different radii with respect to the rotation center given in Soszynski et al. (2003). The results are given in Table 6. As can be seen the dispersion is relatively stable and does not depend on the radius up to the limit of 2.0 degree. We excluded the last bin (2.0–2.5 arcmin) because it contains only 2 objects. Their RV and sigma differ from the values in the other bins, but the sample is too small.

Another test of the dispersion stability is to check the influence of possible outliers. Since the mean V magnitude taken from OGLE and MACHO databases ranges from 18.33 to 21.0

Table 4. Cepheid stars from OGLE, MACHO and EROS database observed with FORS1 and FORS2.

Name	RA	Dec	RV (km s^{-1})	P(days)	V(mag)	Instrument
OGLE LMC-SC7 157350	05:18:33.63	–69:32:15.9	270	2.3425	15.841	FORS2
EROS 2017	05:17:40.78	–69:32:43.1	241	2.4813	15.517	FORS2
OGLE LMC-SC7 165501	05:18:28.17	–69:27:46.1	310	4.3781	15.819	FORS2
EROS 2001	05:17:50.90	–69:28:30.0	263	1.3087	16.983	FORS2
OGLE LMC-SC7 38692	05:17:40.78	–69:32:43.1	211	2.4813	15.517	FORS2
OGLE LMC-SC6 118148	05:20:21.00	–69:12:21.0	259	10.511	17.072	FORS2
OGLE LMC-SC6 102475	05:20:04.63	–69:16:50.9	236	3.3589	15.817	FORS2
MACHO 11.8870.40	05:34:58.00	–70:26:34.8	232	2.9827	16.264	FORS1
MACHO 11.8622.24	05:33:58.00	–70:52:17.4	261	2.0921	15.901	FORS1
MACHO 80.6468.46	05:20:04.00	–69:16:51.2	272	3.3587	15.821	FORS1
MACHO 80.6348.23	05:19:47.00	–69:12:29.8	248	4.7348	15.695	FORS1
MACHO 80.6468.21	05:19:54.00	–69:15:27.4	281	3.1557	15.523	FORS1

Table 5. Observed velocity dispersions.

Population	Number of stars	$RV_{\rm mean}$	$\sigma_{\rm obs}$	$(\sigma^2_{\rm rms} + \sigma^2_{\rm phase})^{-1/2}$	$\sigma_{\rm true}$
LMC Cepheid stars	12	262 ± 8	22 ± 5	16 ± 3	15
LMC LPV stars	73	252 ± 5	35 ± 3	12 ± 2	33
LMC RR Lyrae field stars	137	258 ± 5	57 ± 3	27	50 ± 2
LMC RR Lyrae cluster stars	13	203 ± 6	28 ± 6	27	7 ± 2

Table 6. Mean radial velocity and dispersion as a function of distance from the center of rotation (Soszynski et al. 2003) for RR Lyrae field stars in the LMC.

Radius	N	RV	σ_{RV}
0.0–0.5	43	257	61 ± 7
0.5–1.0	12	247	76 ± 15
1.0–1.5	72	255	49 ± 4
1.5–2.0	9	225	54 ± 9
2.0–2.5	2	316	19 ± 10

(with the average luminosity of the LMC RR Lyrae stars being around $V = 19.4$ mag) the brightest/faintest stars could either not be RR Lyraes or not belong to the LMC. Thus we removed the brightest five and the faintest nine stars and calculated the mean velocity and dispersion using only RR Lyrae stars in the magnitude interval from 18.89 to 19.91. The mean radial velocity and its dispersion is practically the same as for the whole sample: 257 and 57 km s^{-1}, respectively. The velocity dispersion is slightly smaller (55 km s^{-1}), if we take into consideration only 56 stars for which we correct the zeropoint with the skylines (see Sect. 2).

To test if the radial velocity distribution is Gaussian or shows evidence of multiple components we plotted in Fig. 2 the histogram of the radial velocities of RR Lyrae field stars binned to 20 km s^{-1} and the best Gaussian fit to the data. The Kolmogorov-Smirnov test finds that the LMC RR Lyrae star distribution is consistent with a normal distribution with a probability of 99.9% and we have not found evidence for different components.

To measure the rotation we follow the method described in Schommer et al. (1992), Freeman et al. (1983) and Feitzinger & Weiss (1979). First we measured the radial velocities of HI regions using the HI survey performed with the Parkes telescope in Australia (Bruns et al. 2005) at the positions of the centers of our fields. They are given in Col. 3 of Table 7. The observed mean velocities of the RR Lyrae star population in each of the fields is compared with the HI velocity in the same field in the top panel of Fig. 3. The mean radial velocity of the globular cluster NGC 1835 is labeled. The fields LMC-18 and NGC 2019 are excluded from the analysis, because they have only two RR Lyrae stars. They are marked with asterisks. Another three fields LMC-F4 (7 RR Lyrae stars), LMC-7 (5 RR Lyraes) and LMC-F2 (6 RR Lyraes) also have very poor statistics. Equality in Fig. 3 is indicated by the line of slope unity. From the remaining seven fields, two have radial velocities of RR Lyrae stars higher than RV(HI), one with the same RV, and four with RV of the RR Lyrae stars lower than RV(HI). Freeman et al. (1983) compared the HI velocities and the observed velocities of 35 globular

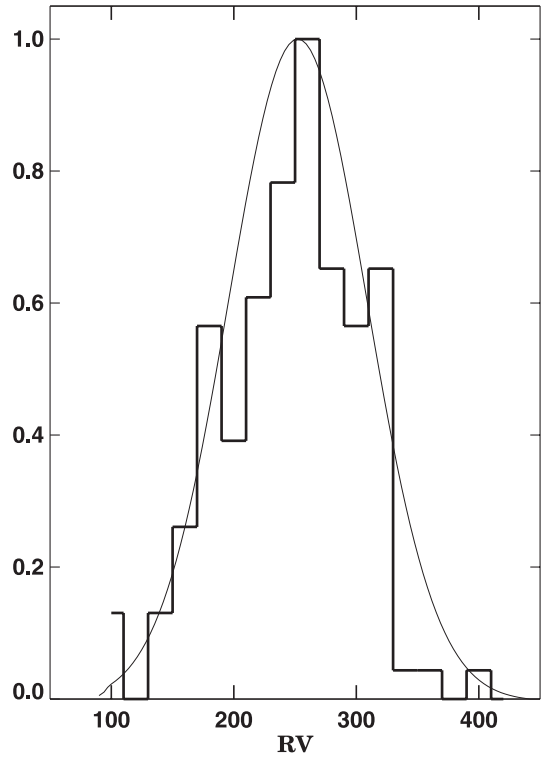

Fig. 2. The radial velocity distributions of RR Lyrae field stars. The solid line represents the best Gaussian fit.

Table 7. Positions and velocities for observed fields in the LMC.

Field	RV	RV(HI)	Radius	X	Y	RV_{cor}	$RV(HI)_{cor}$	PA
LMC-1	264	245	0.69	–0.36	–0.01	81.65	62.65	268
LMC-4	245	245	1.57	–0.12	–1.99	63.05	63.05	184
LMC-7	224	260	1.49	–1.28	–0.80	43.95	79.95	238
LMC-9	263	270	0.03	0.14	–0.46	79.78	86.78	163
LMC-12	237	270	1.94	1.24	–2.10	52.30	85.30	149
LMC-14	259	240	1.67	1.34	–1.67	73.88	54.88	141
LMC-18	316	240	2.77	2.15	–2.48	129.69	53.69	139
Ne01	249	260	0.35	–0.06	–0.71	66.32	77.32	185
LMC-F1	234	260	0.76	0.85	–0.79	49.46	75.46	133
LMC-F2	238	265	1.62	1.59	–1.28	52.20	79.20	129
LMC-F4	328	260	1.45	–1.19	0.01	147.41	79.41	269
NGC1835	198	240	1.38	–1.20	–0.65	17.70	59.70	242
NGC2019	231	265	1.33	1.12	–1.40	28.19	80.19	141

clusters in the LMC. They found that the young and intermediate age globular clusters have the same velocity distribution as the gas, but the older clusters in the LMC have significant systematic offset to lower velocities. We also can see some weak tendency to lower mean velocities of RR Lyrae stars than HI ones, but our data are not enough to outline it.

We transformed equatorial coordinates RA and Dec of our fields to the rectangular X,Y system using equation 1 of Feitzinger & Weiss (1979) with the origin of the coordinate system the center of the LMC as defined by the HI map (RA = $5^{\rm h}20\overset{\rm m}{.}39.84$, Dec = $-69°14'9.5$). This is shown in the second panel of Fig. 3. The position angle (PA) was calculated within this coordinate system, and it increases from N through E. The differences between the radial velocities of the observed fields and HI radial velocities do not show a trend with position angle. We transformed the observed heliocentric radial velocities of the RR Lyrae populations in our fields and of HI to the galactocentric system, using 220 km s^{-1} (van der Marel et al. 2002) for the Galactic rotation. These radial velocities are given in Cols. 7 and 8 of Table 7. To study the rotational properties of RR Lyrae stars we fit the equation from Schommer et al. (1992):

$$V(\theta) = V_{\rm m}[\tan(\theta - \theta_0) \times \sec(i)]^2 + 1^{-0.5} + V_{\rm sys}$$

where $V_{\rm m}$ is the amplitude of the rotation velocity, θ_0 is the orientation of the line of nodes, and $V_{\rm sys}$ is the systemic velocity, while i is the inclination angle, equal to 34.7 (van der Marel et al. 2002). The best fit rotation solution for HI velocities is obtained for $V_{\rm m}$ = 32, $V_{\rm sys}$ = 49 and θ_0 = 172. For RR Lyrae velocities it was not possible to obtain an adequate fit. One reason could be that the mean velocities are less precise than the velocity dispersion or that our fields extend only over the position angles from 120 to 260 degrees.

4. Metallicities

The metallicities are measured using the Gratton et al. (2004) method, which calibrate the so called metallicity index using spectra of variable and constant HB stars of two globular clusters, M 68 and NGC 1851. We used the metallicity calibrations described by Eqs. (3), (4), (5) and (6) of Gratton et al. (2004) and the derived values are listed in Col. 5 of Table 9. We estimate a global uncertainty of 0.20 dex ± 0.02 in the metallicity as a mean value of 18 stars observed with GMOS for which we measured the metallicities on the individual, not summed spectra. The error of this value was calculated as the standard deviation of the mean uncertainty divided by the square root of the number of the stars.

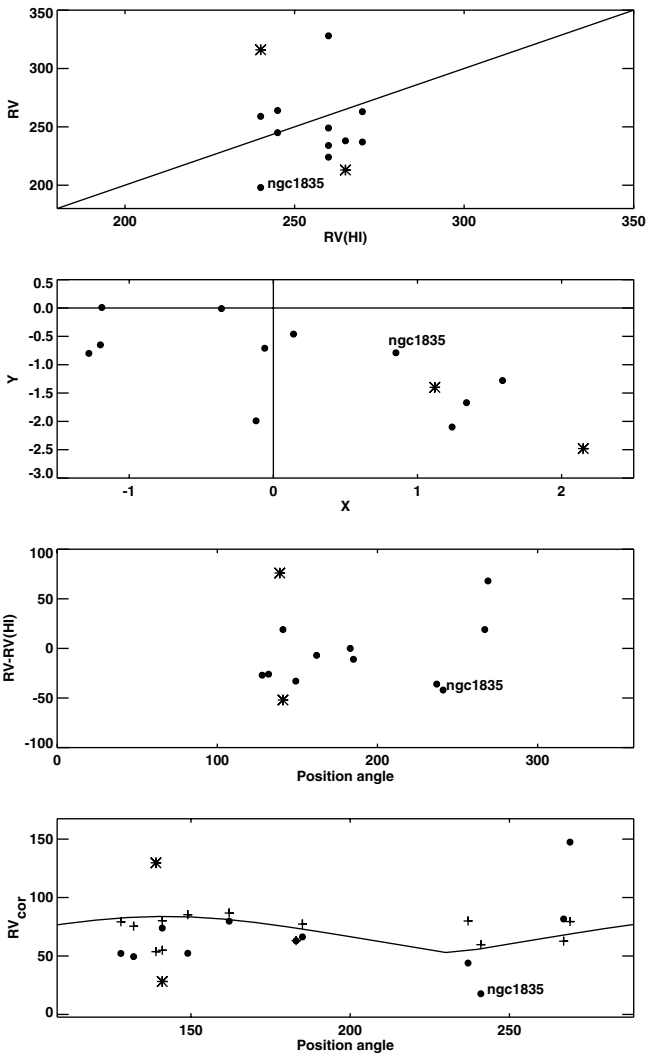

Fig. 3. *Top panel*: the mean radial velocity (RV) of the observed RR Lyrae field stars vs. radial velocity of HI. The mean radial velocity of the RR Lyrae globular cluster NGC 1835 stars is labeled. The asterisks mark the fields LMC-18 and NGC 2019, which are excluded from the analysis (see the text). The solid line is the line of equality. *Second panel*: the rectangular X, Y coordinates in degrees of the observed fields. *Third panel*: the position angle vs. differences between the radial velocities of the observed fields and HI radial velocities. *Bottom panel*: the position angle vs. galactocentric velocities of RR Lyrae stars (points) and HI (crosses). The best fit rotation solution for HI velocities is shown as a solid line.

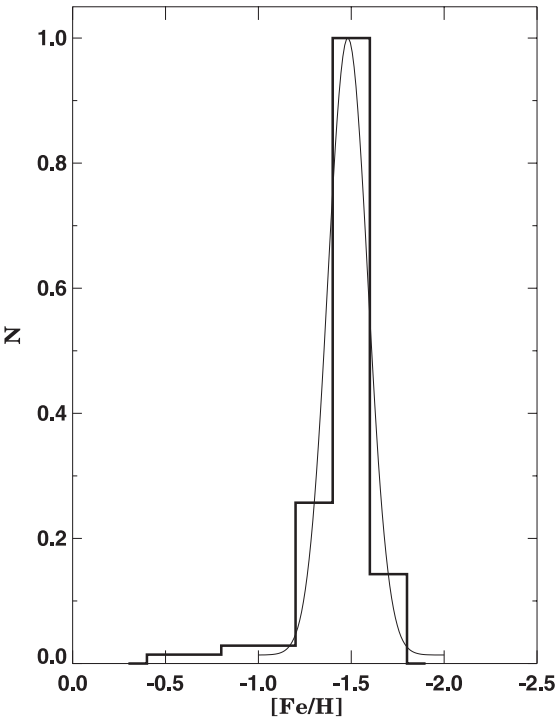

Fig. 4. The metallicity histogram for RR Lyrae stars in our fields. The solid line represents the Gaussian distribution.

Table 8. Mean radial velocity and dispersion for different metallicity bins for field RR Lyrae stars in the LMC.

[Fe/H]	N	RV	σ_{RV}
–0.5–-1.0	3	199	30 ± 17
–1.0–-1.5	21	248	51 ± 11
–1.5–-2.0	80	260	57 ± 6

The average [Fe/H] value of our 104 field RR Lyrae stars is [Fe/H] = −1.53 ± 0.02 dex, which is in good agreement with the Clementini et al. (2003) and Gratton et al. (2004) average value of [Fe/H] = −1.48 ± 0.03 dex. These metallicities are on the Harris (1996) metallicity scale and are on average 0.06 dex more metal-rich than the Zinn and West (1984) scale (Gratton et al. 2004).

The mean metallicity of 5 RRe stars is [Fe/H] = −1.52 ± 0.09 dex, 26 RRc stars have [Fe/H] = −1.53 ± 0.02 dex and 73 RRab stars have [Fe/H] = −1.54 ± 0.03 dex. Therefore we confirm that there are no metallicity differences among Bailey's types (Gratton et al. 2004). The average metallicity of NGC 1835 is [Fe/H] = −1.98 ± 0.06 dex. Thus, the field RR Lyrae stars seem to be more metal rich than globular cluster RR Lyrae stars.

The metallicity distribution of all the field RR Lyrae stars is shown in Fig. 4 and is well fitted by the Gaussian distribution centered on [Fe/H] = −1.48.

In Table 8 we report the mean velocity (RV) and dispersion (σ_{RV}) of different metallicity bins. The dispersion seems to be stable and does not depend on the metallicity. The first metallicity bin shows lower mean radial velocity and dispersion, but the sample is very small – this bin contains only 3 stars. This is in contrast to the result of Cole et al. (2005), who found that the most metal poor RGB stars show higher velocity dispersion. However, they investigated different stellar populations, while in our work we have analyzed the RR Lyrae population in different metallicity bins.

5. Summary and conclusions

We have presented new low-resolution spectra for 100 RR Lyrae field stars in the Large Magellanic Cloud. This sample more than triples that presented in Paper I and allows us to strengthen our previous results regarding the kinematics and metallicity properties of this old and metal-poor population in our nearest neighboring galaxy.

The average metallicity of the whole sample of RR Lyrae stars in the LMC is [Fe/H] = −1.53 ± 0.02 dex. The metallicity distribution is well fitted by a single Gaussian. There is no significant variation of the velocity dispersion with metallicity. This is at odds with the results of Cole et al. (2005) who found an increasing velocity dispersion with decreasing metallicity. However, these authors looked at different stellar populations in the LMC, while our sample comprises only RR Lyrae stars. Thus the trend between the metallicity and velocity dispersion may be due to age rather than to metallicity.

Our main result is that the mean velocity dispersion of the LMC field RR Lyrae stars is $\sigma_{RV} = 50 \pm 2$ km s^{-1}. This quantity does not appear to vary with distance from the LMC center up to 2 degrees.

The mean velocities show some field to field variation, and our conclusions are weaker for this quantity. They appear to differ slightly from the velocities of the HI gas, but our data do not allow us to measure the bulk rotation.

Acknowledgements. D.M. is supported by Fondap Center for Astrophysics 15010003 and by a Fellowship from the John Simon Guggenheim Foundation. We thank our referee, Dr. Gisella Clementini, for very useful comments which helped to improve this manuscript significantly.

References

Alcock, C., Allsman, R. A., Axelrod, T. S., et al. 1996, AJ, 111, 1146
Alcock, C., Allsman, R. A., Alves, D. R., et al. 2000a, ApJ, 542, 281
Alcock, C., Allsman, R., Alves, D. R., et al. 2000b, AJ, 542, 257
Alves, D. R. 2004, Wide Field Imaging from Space, (for New Astronomy Reviews), ed. T. McKay, A. Fruchter, & E. Linder [arXiv:astro-ph/0408336]
Borissova, J., Minniti, D., Rejkuba, M., Alves, D., Cook, K., & Freeman, K. C. 2004, A&A, 423, 97, Paper I
Bruns, C., Kerp, J., Staveley- Smith, L., et al. 2005, A&A, 432, 45
Clementini, G., Gratton, R., Bragaglia, A., et al. 2003, AJ, 125, 1309
Cole, A., Tolstoy, E., Gallanger, J., & Smecker-Hane, T. 2005, AJ, 129, 1465
Feitzinger, J., & Weiss, G. 1979, 37, 575
Dubath, P., Meylan, G., & Mayor, M. 1997, A&A, 324, 505
Freedman, W., Madore, B., Gibson, B., et al. 2001, AJ, 553, 47
Freeman, K. C., Illingworth, G., & Oemler, A., Jr. 1983, ApJ, 272, 488
Gallart, C., Martinez-Delgado, D., Gomez-Flechoso, M. A., & Mateo, M. 2001, AJ, 121, 2572
Gallart, C., Stetson, P., Hardy, E., Pont, F., & Zinn, R. 2004, ApJ, 614, L109
Gratton, R., Bragaglia, A., Clementini, G., Carretta, E., Di Fabrizio, L., et al. 2004, A&A, 421, 937
Harris, W. 1996, AJ, 112, 1487
Layden, A. 1994, AJ, 108, 1016
Minniti, D., Borissova, J., Rejkuba, M., et al. 2003, Science, 301, 1508
Oke, J. B. 1966, ApJ, 145, 468
Schommer, R., Olszewski, E., Suntzeff, N., & Harris, H. 1992, AJ, 103 447
Soszynski, I., Udalski, A., Szymanski, M., et al. 2003, Acta Astron., 53, 93
Subramaniam, A. 2006, A&A, 449, 101
van der Marel, R. P., Alves, D. R., Hardy, E., & Suntzeff, N. B. 2002, AJ, 124, 2639
Vivas, A., Zinn, R., & Gallart, C. 2005, AJ, 129, 189
Zebrun, K., Soszynski, I., Wozniak, P. R., et al. 2001, Acta Astron., 51, 317
Zinn, R., & West, M. J. 1984, ApJS, 55, 45

Online Material

Table 9. The whole sample of the LMC RR Lyrae stars taken with FORS1, FORS2 and GMOS.

Name	RV (km s^{-1})	$\sigma(RV)$	S/N	[Fe/H]	V	Period(d)	Type
MACHO10.3802.311	234	20	38	–1.51	18.99	0.5460	RRab
MACHO10.3802.339	243	25	25	–1.64	19.37	0.5120	RRab
MACHO10.3802.446	165	21	17	–1.60	19.49	0.3080	RRc
MACHO10.3922.978	273	31	27	–1.87	19.09	0.5568	RRab
MACHO10.3923.351	204	40	22	–1.60	19.24	0.3339	RRc
MACHO11.8622.757	263	33	26	–1.59	19.11	0.6860	RRab
MACHO11.8623.3792	221	12	32	–1.49	19.31	0.6149	RRab
MACHO11.8623.779	171	23	32	–1.54	19.20	0.6150	RRab
MACHO11.8623.826	290	14	21	–1.57	18.95	0.5920	RRab
MACHO11.8744.658	197	18	37	–1.52	18.92	0.4155	RRc
MACHO11.8744.752	195	8	29	–1.56	19.14	0.2809	RRe
MACHO11.8744.830	325	23	30	–1.53	19.47	0.5510	RRab
MACHO11.8749.1208	269	27	28	–1.56	19.56	0.4757	RRab
MACHO11.8749.1324	116	38	32	–	19.63	0.5120	RRab
MACHO11.8750.1425	261	26	38	–1.52	19.26	0.3487	RRc
MACHO11.8750.1672	208	24	24	–1.51	19.62	0.3400	RRc
MACHO11.8750.1827	252	16	35	–1.60	19.74	0.5186	RRab
MACHO11.8750.2045	299	19	32	–1.82	19.81	0.4763	RRab
MACHO11.8870.1275	274	16	37	–1.60	19.33	0.4638	RRab
MACHO11.8871.1096	308	11	23	–	19.43	0.5473	RRab
MACHO11.8871.1122	256	32	24	–1.49	19.71	0.5014	RRab
MACHO11.8871.1299	277	28	26	–1.49	19.61	0.5957	RRab
MACHO11.8871.1362	250	17	30	–1.58	19.61	0.6064	RRab
MACHO11.8871.1447	176	16	28	–1.50	19.59	0.2640	RRe
MACHO11.8871.1516	262	15	27	–	19.46	0.5463	RRab
MACHO13.5839.1023	188	38	25	–0.75	19.66	0.5823	RRab
MACHO13.5840.608	252	30	33	–1.53	19.32	0.5188	RRab
MACHO13.5840.730	258	31	31	–1.79	19.41	0.6215	RRab
MACHO13.5840.768	231	25	28	–1.63	19.65	0.5515	RRab
MACHO13.5960.884	225	21	28	–1.56	19.23	0.3459	RRc
MACHO13.5961.435	319	18	36	–1.51	18.84	0.5088	RRab
MACHO13.5961.511	200	26	22	–1.69	19.1	0.7100	RRab
MACHO13.5961.623	281	22	26	–1.60	19.24	0.6180	RRab
MACHO13.5961.648	293	24	30	–	19.39	0.5670	RRab
MACHO13.5961.720	233	24	22	–0.92	19.42	0.6090	RRab
MACHO13.5962.547	279	28	36	–1.71	19.21	0.6464	RRab
MACHO13.5962.656	288	22	26	–1.65	19.34	0.6090	RRab
MACHO13.6082.701	175	18	24	–	19.41	0.5525	RRab
MACHO13.6082.742	215	24	30	–	19.33	0.5163	RRab
MACHO2.5507.5945	315	19	28	–	19.54	0.6234	RRab
MACHO2.5507.6046	338	22	25	–	19.63	0.4920	RRab
MACHO2.5508.3096	196	32	9	–	19.96	0.5593	RRab
MACHO2.5628.5690	225	24	13	–	19.69	0.6156	RRab
MACHO2.5628.6276	177	38	5	–0.57	19.91	0.4781	RRab
MACHO79.5507.1039	317	31	7	–1.32	19.59	0.5608	RRab
MACHO79.5507.1039	325	27	7	–	19.59	0.5608	RRab
MACHO79.5507.1485	313	22	24	–1.60	19.31	0.6234	RRab
MACHO79.5507.1580	244	35	11	–	19.46	0.9720	RRab
MACHO79.5508.427	279	28	15	–1.66	19.73	0.5593	RRab
MACHO79.5508.534	339	10	31	–1.62	19.52	0.5723	RRab
MACHO79.5508.682	216	27	17	–1.77	19.89	0.7591	RRab

Table 9. continued.

Name	RV (km s^{-1})	$\sigma(RV)$	S/N	[Fe/H]	V	Period(d)	Type
MACHO79.5508.735	268	14	33	–1.54	19.78	0.5057	RRab
MACHO79.5628.1065	236	34	7	–1.24	19.84	0.5305	RRab
MACHO79.5628.1300	248	35	15	–	19.42	0.6160	RRab
MACHO79.5628.1597	274	32	5	–	19.51	0.2812	RRe
MACHO79.5628.1650	187	19	20	–	19.26	0.3389	RRc
MACHO79.5628.2110	259	35	10	–	19.8	0.5260	RRab
MACHO80.6347.1940	290	30	24	–1.09	19.21	0.4083	RRc
MACHO80.6467.2128	295	25	12	–	19.35	0.5805	RRab
MACHO80.6468.1883	277	18	46	–1.51	18.92	0.3346	RRc
MACHO80.6468.2616	268	23	42	–1.64	19.21	0.3684	RRc
MACHO80.6468.2799	207	23	25	–1.79	19.32	0.5731	RRab
MACHO80.6469.1657	207	14	29	–1.61	19.24	0.5804	RRab
MACHO80.6469.1712	321	14	47	–1.53	18.84	0.7720	RRab
MACHO80.6588.1605	294	23	35	–	18.96	0.5237	RRab
MACHO80.6588.2703	353	26	28	–1.60	19.23	0.4794	RRab
MACHO80.6589.2425	278	23	36	–1.62	19.51	0.3497	RRc
OGLE050456.54-692449.0	144	39	5	–2.15	20.00	0.2779	RRe
OGLE050457.92-692419.2	213	31	16	–2.31	19.35	0.6000	RRab
OGLE050458.96-692447.2	196	31	15	–2.05	19.20	0.5157	RRab
OGLE050501.95-692343.5	189	33	15	–1.97	19.31	0.3216	RRc
OGLE050503.49-692319.2	199	30	16	–2.22	19.61	0.3350	RRc
OGLE050505.88-692500.9	218	25	27	–1.94	19.30	0.5462	RRab
OGLE050507.42-692346.6	189	28	22	–1.85	19.26	0.5382	RRab
OGLE050508.49-692330.7	213	28	17	–1.66	19.20	0.3674	RRc
OGLE050509.55-692505.5	244	24	22	–1.9	19.04	0.3591	RRc
OGLE05051028-6845491	350	22	12	–	20.66	0.5234	RRab
OGLE050512.73-692446.5	160	32	15	–2.01	19.32	0.3785	RRc
OGLE050514.52-692412.2	217	33	11	–1.72	19.37	0.5179	RRab
OGLE050516.31-684514.9	339	30	35	–1.79	19.41	0.5815	RRab
OGLE050516.31-684514.9	332	33	20	–	19.41	0.5815	RRab
OGLE050519.07-684522.5	337	14	64	–	18.41	0.4556	RRab
OGLE050542.14-684529.5	314	36	17	–	19.42	0.2679	RRe
OGLE05054491-6844330	319	31	29	–1.84	19.30	0.5132	RRab
OGLE05055814-6846186	304	13	30	–	19.08	0.4897	RRab
OGLE051731.19-692717.7	376	13	24	–1.62	18.93	0.5908	RRab
OGLE051738.47-692628.8	309	33	19	–1.79	19.15	0.6341	RRab
OGLE051751.38-692707.5	118	15	35	–1.61	18.89	0.5229	RRab
OGLE051751.97-692741.4	248	3	32	–1.50	19.50	0.5888	RRab
OGLE051752.63-692856.4	252	23	37	–1.67	19.00	0.6663	RRab
OGLE051755.55-692716.3	294	27	59	–1.56	18.33	0.5738	RRab
OGLE051755.91-693005.5	279	17	20	–1.51	19.22	0.4873	RRab
OGLE051756.52-692934.7	413	28	37	–1.55	19.29	0.3532	RRc
OGLE051756.59-692803.2	225	22	44	–1.53	18.74	0.4076	RRc
OGLE051808.73-692813.4	256	23	27	–1.55	18.98	0.4000	RRc
OGLE051813.74-692840.6	228	23	41	–1.54	19.16	0.6497	RRab

Table 9. continued.

Name	RV (km s^{-1})	$\sigma(RV)$	S/N	[Fe/H]	V	Period(d)	Type
OGLE051815.14-692924.1	233	16	21	–1.55	19.28	0.5306	RRab
OGLE051825.24-692848.6	236	24	22	–	19.44	0.4735	RRab
OGLE051825.32-692651.3	105	28	31	–1.59	19.29	0.5996	RRab
OGLE051831.26-693054.5	155	35	25	–	19.15	0.2743	RRe
OGLE051834.08-693049.0	188	26	20	–	19.18	0.2743	RRc
OGLE051835.21-692913.5	296	29	21	–	19.26	0.2707	RRe
OGLE051842.29-692642.8	277	32	13	–	20.16	0.2901	RRc
OGLE052002.59-691431.1	244	20	30	–1.52	18.96	0.3365	RRc
OGLE052003.29-691316.1	298	16	32	–1.52	18.89	0.5725	RRab
OGLE052005.99-691313.3	180	20	21	–1.52	19.06	0.7525	RRab
OGLE052011.82-691424.0	335	18	25	–1.50	19.4	0.2639	RRe
OGLE052013.42-691153.0	195	23	33	–1.53	18.97	0.6175	RRab
OGLE052018.99-691527.0	321	37	22	–1.62	19.51	0.5739	RRab
OGLE052021.61-691235.9	211	22	20	–1.57	19.28	0.3314	RRc
OGLE052022.42-691202.3	271	28	11	–1.52	19.33	0.7720	RRab
OGLE052026.29-691815.0	224	14	41	–1.50	19.12	0.3702	RRc
OGLE052027.12-691607.1	181	34	32	–1.53	19.18	0.5844	RRab
OGLE052030.65-691345.2	199	22	21	–1.50	19.10	0.3494	RRc
OGLE052032.64-691701.6	240	28	24	–1.60	19.33	0.3330	RRc
OGLE052033.36-691334.2	284	25	19	–1.54	19.23	0.5805	RRab
OGLE052039.40-691709.0	283	26	18	–1.52	19.05	0.2761	RRe
OGLE052043.39-691742.7	331	23	20	–1.57	19.34	0.4794	RRab
OGLE052044.57-691726.3	258	33	17	–1.54	19.32	0.3497	RRc
OGLE052811.62-693423.8	321	38	29	–	19.50	0.5385	RRab
OGLE052822.65-693529.9	304	26	26	–1.64	19.42	0.5210	RRab
OGLE052822.98-693310.6	319	27	28	–1.62	19.40	0.5800	RRab
OGLE052827.10-693347.7	198	38	14	–1.47	20.06	0.4195	RRc
OGLE052829.20-693201.1	149	20	39	–1.35	19.30	0.6023	RRab
OGLE052829.28-693442.0	252	23	33	–1.43	19.80	0.5755	RRab
OGLE052834.72-693326.4	149	16	36	–1.58	19.37	0.6055	RRab
OGLE052854.41-693403.8	184	28	34	–1.32	19.40	0.6214	RRab
OGLE053156.19-700954.7	234	15	65	–	18.72	0.5739	RRab
OGLE053159.01-700959.3	228	30	32	–	19.31	0.5069	RRab
OGLE053411.38-702413.4	220	33	29	–1.54	19.4	0.3400	RRc
OGLE053416.61-702149.6	287	25	41	–1.51	19.26	0.3315	RRc
OGLE053418.91-702309.6	308	38	19	–1.60	19.59	0.5188	RRab
OGLE053427.44-702249.8	335	22	21	–1.62	19.48	0.4764	RRab
OGLE053437.49-702806.9	180	32	22	–	19.25	0.4757	RRab
OGLE053443.15-702543.8	271	22	23	–1.50	19.39	0.2948	RRe
OGLE053459.49-702232.9	263	18	25	–1.61	19.35	0.5473	RRab
OGLE053500.75-702533.0	277	21	24	–1.53	19.48	0.5014	RRab
OGLE053502.87-702829.6	332	29	32	–1.50	19.36	0.3286	RRc
OGLE053504.52-702444.9	277	24	16	–1.68	19.35	0.5958	RRab
OGLE053509.25-702145.7	248	21	23	–1.55	19.28	0.3587	RRc
OGLE053510.95-702729.9	224	30	7	–	21.00	0.6274	RRab
OGLE053518.04-702755.2	301	33	15	–	19.35	0.5134	RRab
OGLE053713.07-695956.8	270	21	12	–1.10	19.98	0.6161	RRab
OGLE053714.30-695846.0	278	28	17	–1.38	20.00	0.6502	RRab
OGLE053715.52-695812.2	214	28	15	–1.41	20.08	0.5353	RRab
OGLE053715.59-700105.8	251	34	5	–	21.00	0.5642	RRab
OGLE053717.79-695923.9	178	23	32	–1.60	19.57	0.2869	RRc
OGLE053720.10-700202.5	291	33	31	–1.39	19.51	0.7042	RRab
OGLE054527.55-710615.3	329	25	11	–	19.89	0.7787	RRab
OGLE054600.10-711155.3	302	31	28	–1.71	19.31	0.5711	RRab